The Journal of Experimental Medicine

Adiposity induces lethal cytokine storm after systemic administration of stimulatory immunotherapy regimens in aged mice

Annie Mirsoian,[1]* Myriam N. Bouchlaka,[1]* Gail D. Sckisel,[1] Mingyi Chen,[2] Chien-Chun Steven Pai,[1] Emanuel Maverakis,[1] Richard G. Spencer,[5] Kenneth W. Fishbein,[5] Sana Siddiqui,[5] Arta M. Monjazeb,[3] Bronwen Martin,[5] Stuart Maudsley,[5] Charles Hesdorffer,[5] Luigi Ferrucci,[5] Dan L. Longo,[5] Bruce R. Blazar,[6] Robert H. Wiltrout,[7] Dennis D. Taub,[4,8]** and William J. Murphy[4]**

[1]Department of Dermatology, [2]Department of Pathology and Laboratory Medicine, [3]Department of Radiation Oncology, and [4]Department of Dermatology and Internal Medicine, University of California, Davis, Sacramento, CA 95817
[5]National Institute on Aging-Intramural Research Program, National Institutes of Health, Biomedical Research Center, Baltimore, MD 21224
[6]Division of Blood and Marrow Transplantation, Department of Pediatrics, University of Minnesota, Minneapolis, MN 55455
[7]National Cancer Institute, Frederick, MD 21702
[8]Hematology and Immunology Translational Research Center, VA Medical Center, Washington, DC 20422

Aging is a contributing factor in cancer occurrence. We recently demonstrated that systemic immunotherapy (IT) administration in aged, but not young, mice resulted in induction of rapid and lethal cytokine storm. We found that aging was accompanied by increases in visceral fat similar to that seen in young obese (*ob/ob* or diet-induced obese [DIO]) mice. Yet, the effects of aging and obesity on inflammatory responses to immunotherapeutics are not well defined. We determine the effects of adiposity on systemic IT tolerance in aged compared with young obese mice. Both young *ob/ob*- and DIO-generated proinflammatory cytokine levels and organ pathologies are comparable to those in aged ad libitum mice after IT, culminating in lethality. Young obese mice exhibited greater ratios of M1/M2 macrophages within the peritoneal and visceral adipose tissues and higher percentages of TNF+ macrophages in response to αCD40/IL-2 as compared with young lean mice. Macrophage depletion or TNF blockade in conjunction with αCD40/IL-2 prevented cytokine storms in young obese mice and protected from lethality. Calorie-restricted aged mice contain less visceral fat and displayed reduced cytokine levels, protection from organ pathology, and protection from lethality upon αCD40/IL-2 administration. Our data demonstrate that adiposity is a critical factor in the age-associated pathological responses to systemic anti-cancer IT.

CORRESPONDENCE
William J. Murphy:
wmjmurphy@ucdavis.edu

Abbreviations used: AL, ad libitum; ALT, alanine aminotransferase; CR, calorie restricted; DIO, diet-induced obese; HD, high dose; IT, immunotherapy; LD, low dose; MRI, magnetic resonance imaging.

The use of immunotherapy (IT) in cancer has recently resulted in impressive responses. Yet, the usages of IT regimens, especially those involving cytokine therapies, have also resulted in the induction of severe systemic toxicities often not previously characterized in their preclinical animal studies. Because such toxicities often require intensive care management of patients, the causes for the discrepancies in observations between clinical and preclinical toxicity merit further study.

Cancer has been considered a disease of aging, with persons over 65 accounting for over 60% of newly diagnosed malignancies (Balducci and Ershler, 2005). Consequences of aging include gradual decreases in immunological function, thymic involution leading to decreased naive T cell output, restriction within T cell repertoire

*A. Mirsoian and M.N. Bouchlaka contributed equally to this paper.
**D.D. Taub and W.J. Murphy contributed equally to this paper.

The Rockefeller University Press $30.00
J. Exp. Med. 2014 Vol. 211 No. 12 2373–2383
www.jem.org/cgi/doi/10.1084/jem.20140116

2373

diversity, increases in genomic instability, and increases in cellular senescence (Campisi, 2013). However, despite the majority of patients being of this demographic, the overwhelming majority of preclinical studies are performed in young inbred mice. We recently demonstrated that treatment of young mice with a combination IT regimen consisting of agonistic monoclonal antibody to CD40 (αCD40) given in conjunction with IL-2 resulted in synergistic anti-tumor effects and was well tolerated (Murphy et al., 2003). Yet, administration of the same regimen in an aged cohort resulted in 100% lethality within two days of treatment (Bouchlaka et al., 2013). Importantly, the mortality in the aged was perpetuated by an aberrant cytokine storm mirroring a systemic inflammatory response syndrome (SIRS), which resulted in multi-organ damage (Bouchlaka et al., 2013). These systemic toxicities were closely representative of those previously noted clinically with FDA-approved immunostimulatory IT therapeutics such as high-dose IL-2 and IFN-α (Lee and Margolin, 2011).

Aging is associated with a gradual decline in immunological function but is also accompanied by the coincidence of a systemic, chronic, and low-grade proinflammatory response termed inflammaging that leads to increased systemic cytokine levels, namely IL-1β, IL-6, and TNF (Franceschi, 2007). Emerging data suggests that inflammaging may be influenced by age-associated changes in body mass composition such as decreased lean muscle mass, increased adiposity, and increases in overall body mass index (BMI; Franceschi et al., 2000). Whether adiposity plays a role in the generation of systemic toxicities or whether it is primarily an age-associated occurrence remains unknown.

Like aging, hallmark to the obese microenvironment is the development of a low-grade chronic "meta-inflammatory" state. Excess adiposity is associated with increased infiltration of macrophages and proinflammatory mediators such as dendritic cells, NK cells, and T cells into fat depots that ultimately results in environmental remodeling. Consequences include increased circulating levels of C-reactive protein (CRP), IL-6, leptin, and TNF (Ronti et al., 2006; Vázquez-Vela et al., 2008). Importantly, the immunomodulatory effects of increased adipose tissue extends through the ability for both adipocytes and the stromal vascular fraction to express a variety of immunologically important surface receptors, such as the leptin receptor, IL-6 receptor, and both p55 and p75 TNF receptors (Ailhaud, 2000). Systemic consequences of increased adiposity are also seen at distance sites through premature induction of aging-associated changes such as thymic involution, which leads to the restriction of naive T cell output and ultimately restriction of the T cell repertoire (Yang et al., 2009).

Collectively, the field of IT has made great progress in the last decade toward the development of therapeutic candidates against cancer. Yet, these candidates have been met in the clinic with the induction of severe, often limiting, systemic toxicities that hinder their usage. Additionally, given the rise of obesity within society, as well as the estimation that cancer is a disease primarily of the aged, using lean and young models may not accurately reflect patient outcomes. Therefore, this study seeks to establish the consequences of increased adipose tissue accumulation throughout aging upon IT-induced toxicities. Here, we find that adiposity results in a skewing toward increased levels of proinflammatory M1 macrophages within the peritoneal cavity and visceral adipose tissues that ultimately result in heightened production of proinflammatory cytokines, namely TNF, during strong immune stimulation with IT. Importantly, aged ad libitum (AL)–fed mice and young obese mice succumb to TNF-mediated pathological responses culminating in rapid lethality, which are prevented through caloric restriction in the aged or through either macrophage depletion or TNF blockade.

RESULTS

IT administration in the aged results in rapid lethal cytokine storm and is associated with increased accumulation of visceral adipose tissue

The combination IT regimen consisting of αCD40 and IL-2 (αCD40/IL-2) has previously shown synergistic anti-tumor effects resulting in the regression of metastatic tumors in young (<6 mo) mouse models (Murphy et al., 2003). Recently, we demonstrated that administration of the therapeutic dose (high dose [HD]) of αCD40/IL-2 into aged mice (≥15 mo) resulted in a heightened cytokine storm that prompted multi-organ damage and resulted in 100% lethality by day 2 of treatment (Bouchlaka et al., 2013). To address whether the increased lethality was specific to this therapeutic dosage in the aged, we administered αCD40/IL-2 at a lower dose (LD), less than half, into aged AL-fed mice. Consistent with our previous findings, treatment of aged mice with LD IT resulted in 100% mortality by day 2 of treatment (Fig. 1 A) and demonstrated increased serum levels of proinflammatory cytokines TNF, IL-6, and IFN-γ, indicative of a cytokine storm (Fig. 1 B). In addition, to ensure that the lethality observed in the aged mice was not IT regimen–specific, we administered an IT combination of CpG and IL-2 (CpG/IL-2) into young WT and aged AL mice. Confirming our previous findings, aged mice treated with CpG/IL-2 therapy incurred a similar cytokine storm that culminated in rapid lethality by day 3 (Fig. 1, C–E), in contrast to young mice which exhibited lower levels of cytokines and demonstrated complete treatment tolerance (Fig. 1, C–E).

Normal aging is inherently associated with changes in body mass composition—specifically with decreases in muscle mass and increases in intra-abdominal visceral adiposity (Harris, 2002). Equally, within our animal studies an observable difference between aged and young mice is noted in overall size, in particular increased waist circumference (Fig. 1 F). On average, aged mice weigh twice as much as young (Fig. 1 G). To determine whether the difference in size is due to increases in fat deposits, we sought to quantify differences in body mass and the presence of visceral adiposity. Young (<6 mo) and aged (≥15 mo) C57BL/6 mice were analyzed through magnetic resonance imaging (MRI) to quantify the presence of visceral adiposity. Aged mice exhibited markedly increased body mass indices and total visceral fat volumes in comparison with young
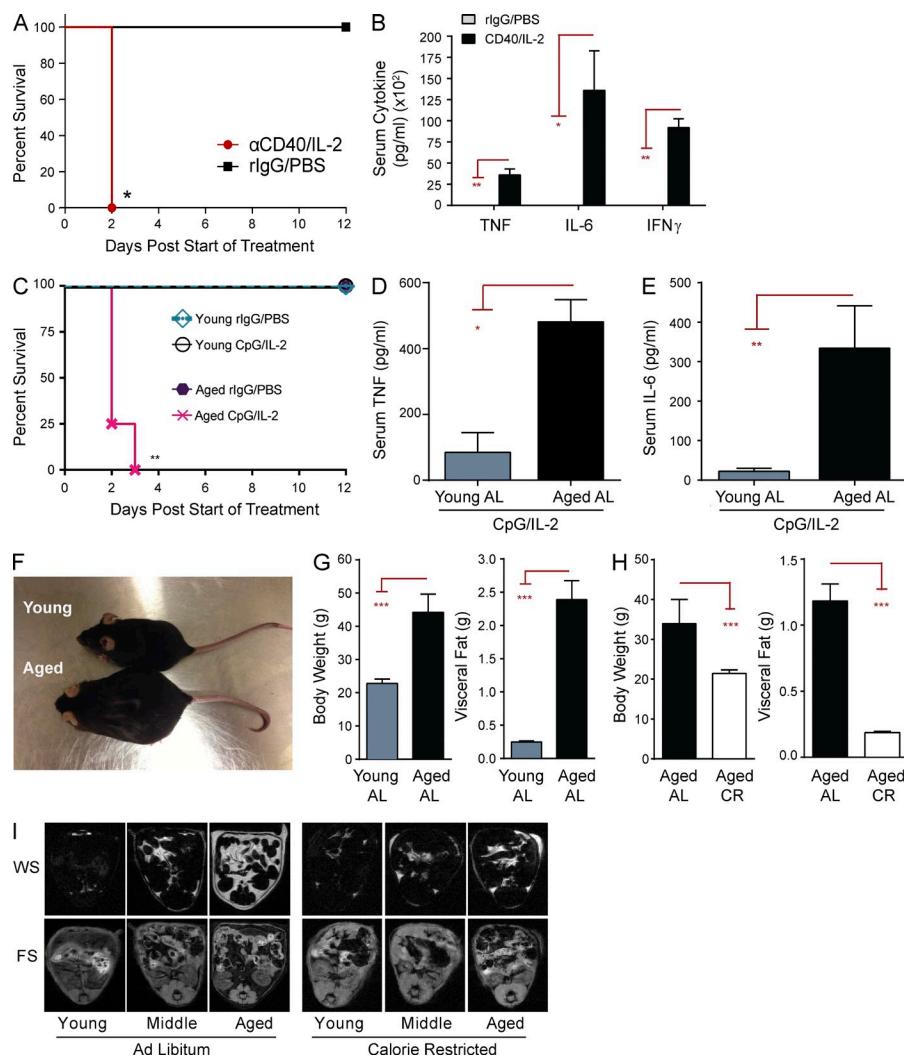
Figure 1. Aged AL mice show increased proinflammatory cytokines, rapid lethality to LD IT, and display increased fat volume ratios in comparison to aged CR mice. (A) Ad libitum–fed C57BL/6 mice were treated with LD αCD40/IL-2 or rIgG/PBS and survival was monitored, n = 5–8 mice/group. (B) Serum cytokines TNF, IL-6, and IFN-γ were measured day 2 by CBA after the start of αCD40/IL-2 or rIgG/PBS therapy in aged AL mice, n = 3–5 mice/group. (C) Young AL (3 mo) and aged AL (18 mo) mice were treated with CpG/IL-2 IT and survival was monitored, n = 5 mice/group. (D and E) Serum cytokine levels of TNF (D) and IL-6 (E) were measured by CBA on day 2 after the start of therapy, n = 5 mice/group. (F) Representative image of aged and young C57BL/6 mice showing size and waist circumference. (G) Total body weight (left graph) and visceral fat weight (right graph), was measured for young (2 mo) and aged AL mice (20 mo), n = 5 mice/group. (H) Total body weight (left graph) or visceral fat (right graph) was measured in naive 15-mo-old C57BL/6 mice on an AL or CR diet, n = 3–4 mice/group. (I) Visceral fat in young (4 mo), middle-aged (9 mo), and aged (15 mo) mice on either an AL (left) or CR (right) diet was evaluated by MRI. WS is indicative of water suppression, where fat is bright. FS is indicative of fat suppression, fat is dark/black. Data in all panels are representative of one of at least five experiments with similar results. MRI scans are representative of one of at least three mice imaged per group with similar results. Survival analysis was plotted according to the Kaplan-Meier method, and statistical differences were determined with the log-rank test. Bar graph (mean value ± SEM) statistics were performed using either one-way or two-way ANOVA with Bonferroni post-hoc tests. ***, P < 0.001; **, P < 0.01; *, P < 0.05.

mice (Fig. 1, G and I). These results indicate that aged mice are not only heavier and larger in size but that these size differences are attributed to increases in adipose tissue accumulation.

Adipose tissue is widely published to be a highly active metabolic organ with immune modulatory capabilities. To address whether in our aged AL-fed mice, who were allowed to freely access food, the increased adiposity noted was contributory toward the development of IT-induced toxicities in the aged, we aimed to determine the effects of IT administration into an aged calorie-restricted (CR) cohort. CR mice are placed on a food restriction diet beginning at 14 wk of age and maintained throughout life. To ensure that age-matched CR aged mice contained a decreased accumulation of body fat in comparison with aged AL mice, we quantified total body weight and visceral fat through MRI (Fig. 1, H and I). CR mice weighed significantly less than AL aged mice and exhibited a decreased presence of visceral adiposity to levels that

were similar to young mice (Fig. 1, G–I). MRI scans of young (4 mo), middle-aged (9 mo), and aged (15 mo) mice that were either AL-fed or CR throughout life showed significant differences in adipose accumulation over time (Fig. 1 I). We found that with increasing age, AL-fed mice have a proportional increase in body fat content, whereas mice placed on a CR diet lack increased fat accumulation regardless of age. Aged CR mice show no significant difference in fat volume ratios to their middle-age and young counterparts, and remain similar to young AL mice (Fig. 1 I).

Caloric restriction in aged mice results in decreased accumulation of adiposity and protection from IT–induced toxicity

To examine the effect of adiposity and aging on the development of systemic toxicities after IT, aged AL, aged CR, and young AL mice were administered IT or a control therapy
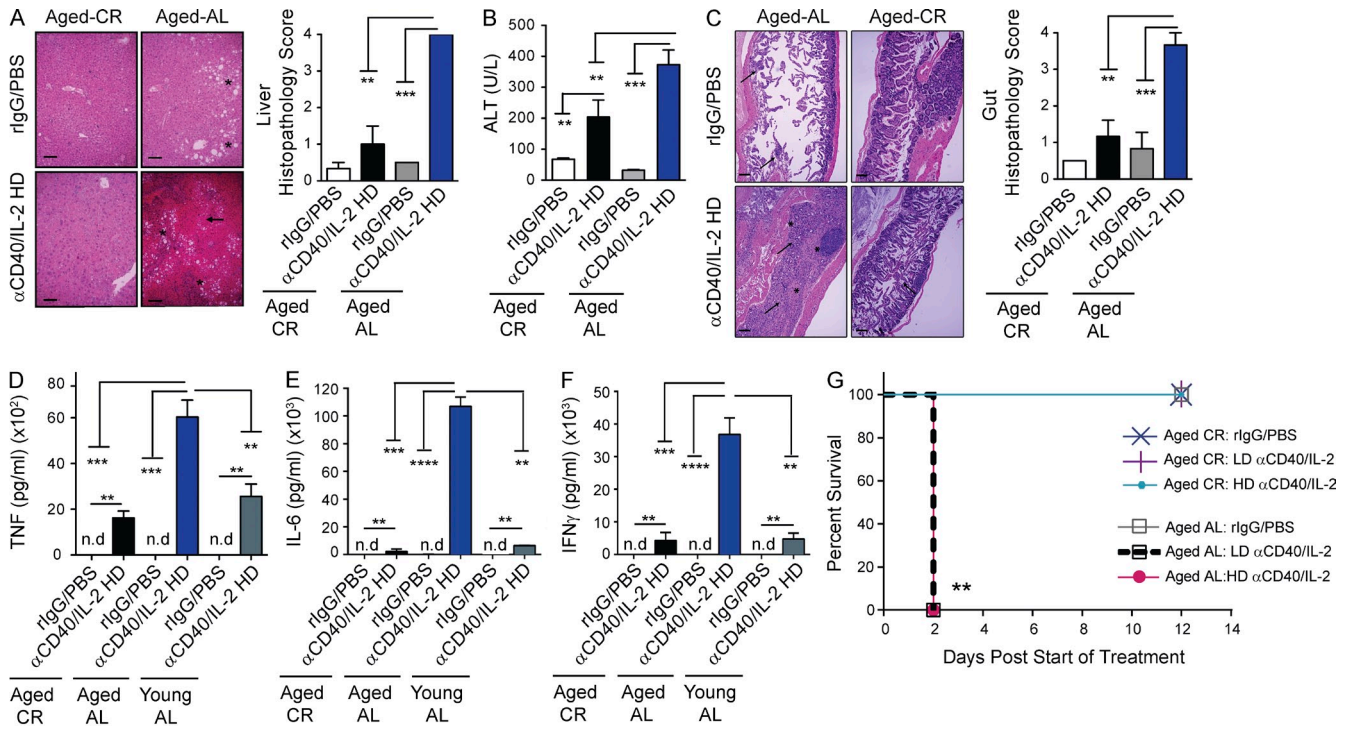
Figure 2.   Calorie restriction in the aged confers protection by decreasing cytokine levels and IT–associated organ pathology, thereby allowing increased survival during IT. (A–C) Aged AL and age-matched aged CR mice (18 mo) were treated with HD αCD40/IL-2 or rIgG/PBS; at day 2 of IT, mice were sacrificed for histological analysis of livers (A) and intestines (C). Serum was collected on day 2 and assessed for ALT (B) levels, *n* = 3 mice/group. Representative H&E images of liver and intestines (gut) for aged AL and aged CR groups. Bars, 200 μm. Asterisks represent steatosis and arrows denote areas of severe immune infiltration and/or necrosis. (D–F) Serum was analyzed day 2 after treatment for TNF (D), IL-6 (E), and IFN-γ (F). (G) Aged (18 mo) C57BL/6 mice on AL or CR diet were treated with either LD or HD of αCD40/IL-2 and survival was monitored. Control groups received rIgG/PBS. All data panels are representative of one of four independent experiments with similar results for all panels. Survival analysis was plotted according to the Kaplan-Meier method and statistical differences were determined by using the log-rank test. Bar graph (mean value ± SEM) statistics were performed using one-way ANOVA with Bonferroni post-hoc test. ****, $P < 0.0001$; ***, $P < 0.001$; **, $P < 0.01$.

(rIgG/PBS). IT resulted in increased lymphocytic infiltrates to the liver of aged CR and aged AL mice, in contrast to age-matched control-treated mice (Fig. 2, A–C). To assess whether IT resulted in organ damage, livers and intestines were collected on day 2 of treatment, the day of mortality in aged AL mice, and assessed for pathological changes. Importantly, livers and intestines from aged CR mice demonstrated significantly less inflammation and less necrosis in comparison with aged AL mice (Fig. 2, A and C). Serum analysis of alanine aminotransferase (ALT) enzyme levels, a correlate of liver damage, showed a significant reduction in ALT levels in aged CR mice in comparison with aged AL mice (Fig. 2 B). Additionally, serum proinflammatory cytokine analysis of TNF (Fig. 2 D), IL-6 (Fig. 2 E), and IFN-γ (Fig. 2 F) resulted in all cytokines being significantly decreased in aged CR mice in comparison with the aged AL mice. These decreases in cytokine values were to levels that were either lower-than or as-low-as those in young AL mice that received IT (Fig. 2, D–F). To determine if these lower cytokine values during IT therapy would confer protection against IT-induced mortality, aged AL mice and aged CR mice were administered either LD IT or HD IT and monitored for mortality. Independent of treatment dose, aged AL mice all

succumb to mortality on day 2 of treatment (Fig. 2 G). However, 100% of aged CR mice placed on the HD amount of IT demonstrated complete protection from αCD40/IL-2–mediated lethality (Fig. 2 G). Collectively, these data suggest that increased body fat plays a critical role in the induction of systemic toxicities by IT. Increased adiposity played a critical role in the age-associated cytokine storm and subsequent organ pathologies after IT and calorie restriction diminished the development of such toxicities conferring a protective effect that allowed for increased survival in the aged.

Increased adipose tissue accumulation through obesity, in the absence of age, results in IT–induced lethal cytokine storm

To further dissect the role of adipose tissue in the IT-associated inflammatory responses seen in aged mice, we next sought to determine the impact of adiposity, in the absence of age, as a possible cofactor. Young *ob/ob* mice (B6.Cg-Lep*ob/ob*) are leptin-deficient and therefore start exhibiting obesity by 3 wk of age. In comparison to age-matched young WT (2 mo) control mice placed on an AL diet (young AL), *ob/ob* mice have significantly higher body masses and weigh, on average, ∼2.5× greater (Fig. 3 A). MRI analysis of body fat content demonstrated
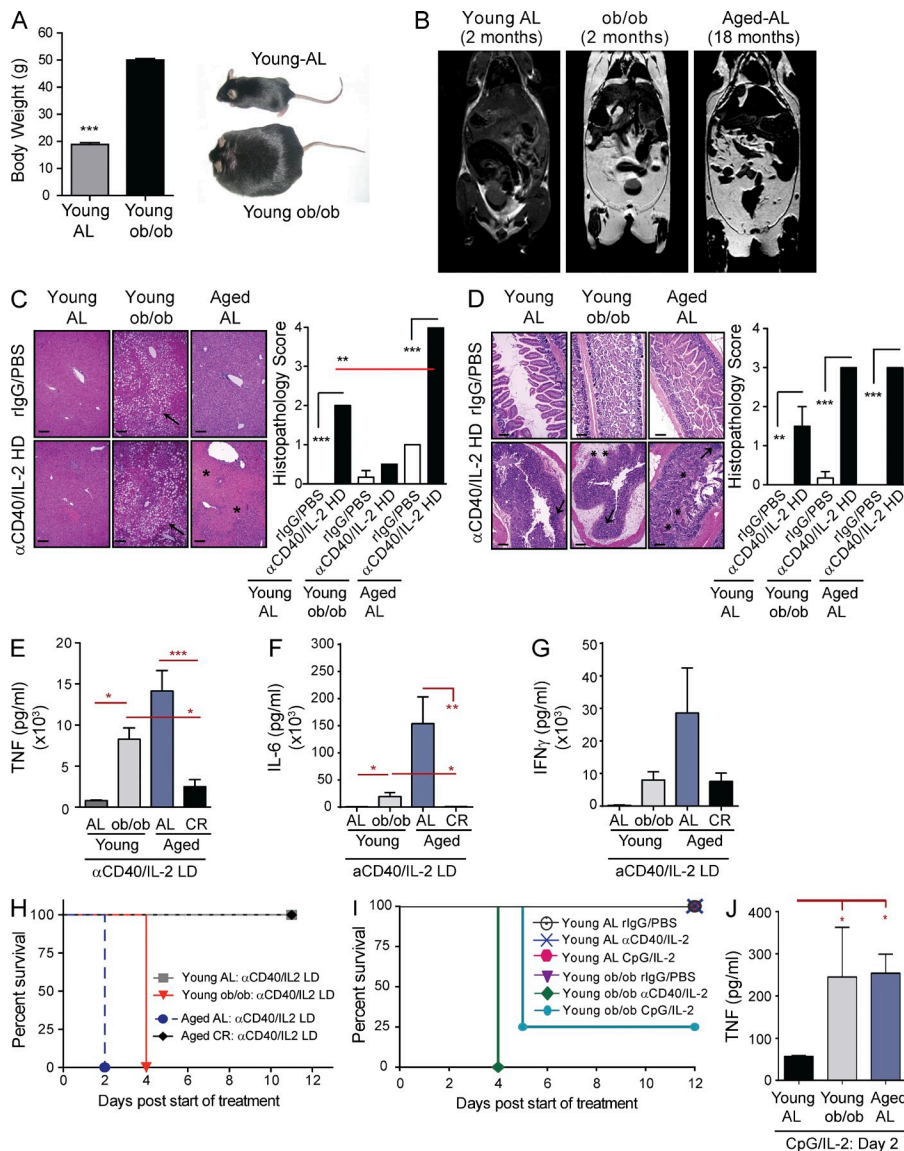
Figure 3. Increased adiposity independently of age results in systemic release of proinflammatory cytokines and organ pathology after IT in young *ob/ob* (obese) and aged AL mice. (A) Body weights of naive young (2 mo) WT and young *ob/ob* C57BL/6 mice, *n* = 6 mice/group. Representative pictures of young-AL WT mice and obese *ob/ob* naive mice are shown. (B) Total fat content in naive young WT (2 mo), young *ob/ob* (2 mo), and aged (18 mo) C57BL/6 mice was visualized by MRI. Fat is bright. (C and D) Young AL (2 mo), young *ob/ob* (2 mo), and aged AL (18 mo) mice were treated with HD αCD40/IL-2 and liver (C) and gut (D) were stained with H&E and scored for histopathology on day 2. Bars, 200 µm. Arrows indicate areas of steatosis and/or immune cell infiltration and asterisks indicate patchy necrosis and/or fibrosis. (E–G) Young AL (2 mo), young *ob/ob* (2 mo), aged AL (18 mo), and aged CR (18 mo) were treated with LD αCD40/IL-2 and serum was collected day 2 of treatment and analyzed by CBA for levels of: TNF (E), IL-6 (F), and IFN-γ (G), *n* = 3 mice/group. (H and I) Young AL (2 mo), young *ob/ob* (2 mo), aged AL (18 mo), and aged CR (18 mo) were treated with LD αCD40/IL-2 (H) or CpG/IL-2 (I) or rIgG/PBS control and survival was monitored. (J) Serum levels of TNF were measured on day 2 of CpG/IL-2 therapy by CBA. Data in all panels are representative of one of at least three experiments with similar results. MRI scans are representative of at least three mice imaged per group with similar results. Survival data were plotted using the Kaplan-Meier method and statistical differences were determined with the log-rank test. Bar graph (mean value ± SEM) statistics performed using Student's *t* test or one-way ANOVA with Bonferroni post-hoc tests. ***, P < 0.001; **, P < 0.01; *, P < 0.05.

that young *ob/ob* mice have higher total body fat content that is similar in accumulation to the aged mice, being deposited largely in the intra-abdominal cavity, in comparison with young AL mice (Fig. 3 B).

To determine if adiposity could solely induce toxic consequences in aged AL, young *ob/ob* and age-matched young AL mice were treated with HD IT and at day 2 of treatment analyzed for the presence of immune-mediated organ pathological changes within the liver and intestines (Fig. 3, C and D). IT resulted in mild inflammatory infiltrates in young AL mice but resulted in moderate to severe inflammation in the o*b/ob* mice, which was comparable to the aged within the intestines (Fig. 3 D). Yet, analysis of IT-induced liver pathology was hindered by the presence of extensive steatosis in *ob/ob* mice, resulting in a paradoxical interference in determining the intensity of immune-mediated inflammatory liver damage (Fig. 3 C). IT resulted in both the intestines and liver displaying the most immune-mediated inflammatory damage within the *ob/ob* that

was comparable to the aged AL mice and significantly greater than the young AL (Fig. 3, C and D).

Because HD IT resulted in significant changes within the obese *ob/ob* mice, we next administered the lower dose (LD) of IT to young *ob/ob*, young age-matched AL mice, aged AL, and aged CR mice. Administration of LD IT still resulted in significant increases in TNF and IL-6 proinflammatory cytokine levels within the young *ob/ob* that were not significantly different to the aged AL mice (Fig. 3, E and F). Both *ob/ob* and aged AL were significantly greater than both the young AL and aged CR mice, where CR in the aged led to significant down-regulation in both TNF and IL-6 cytokine production (Fig. 3, E and F). Although the young *ob/ob* and the aged AL mice displayed increased levels of IFN-γ, these levels were not significant among the groups (Fig. 3 G). Consistent with the increase in proinflammatory cytokines at day 2 of IT treatment, 100% of young *ob/ob* mice succumbed to IT-induced lethality within 4 days of treatment in contrast to 100% survival in the
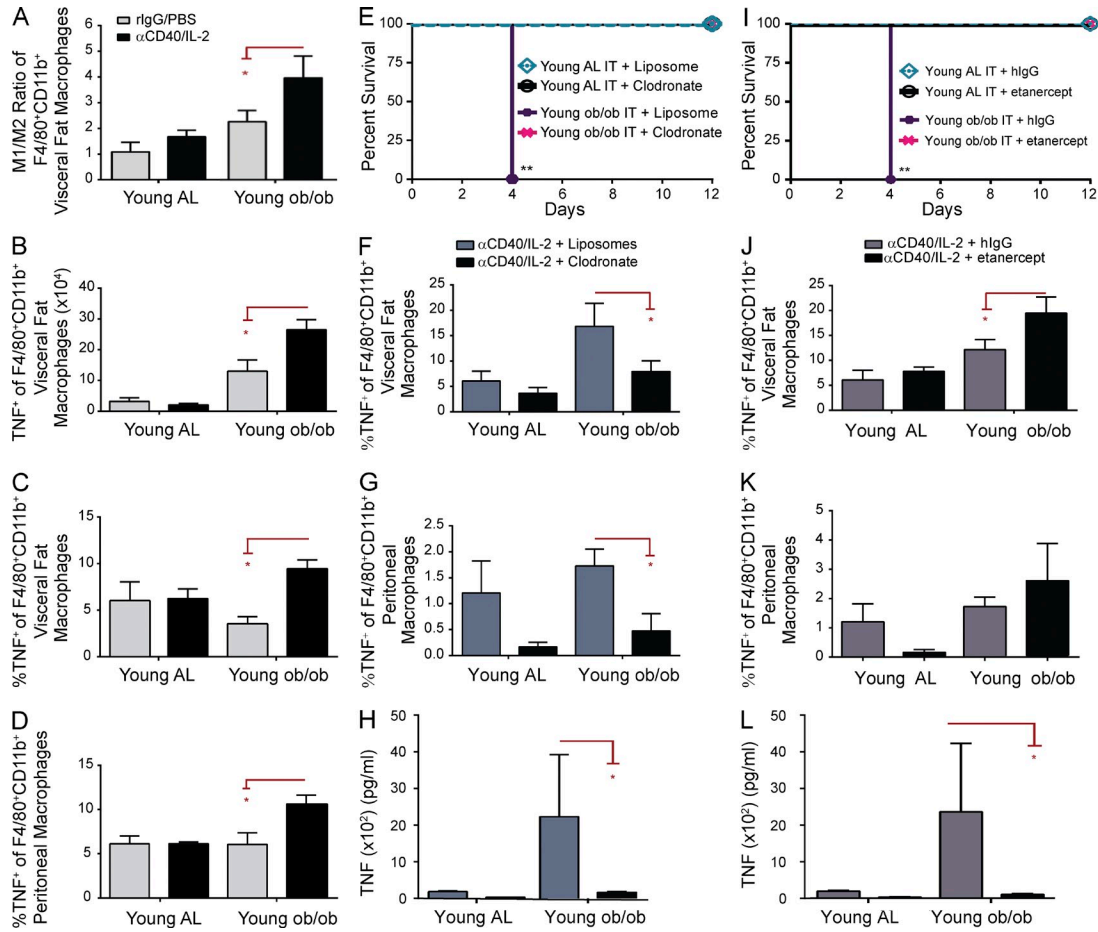
Figure 4. IT toxicity is TNF–dependent through M1 macrophage accumulation. (A–D) Young (2 mo) WT and young (2 mo) *ob/ob* mice were treated with either control rIgG/PBS or LD αCD40/IL-2. Visceral adipose tissue and peritoneal lavages were collected on day 2 and assessed for the presence of macrophages identified as CD45+CD19−F4/80+CD11b+. Ratio of M1/M2 macrophages (A), and total numbers (B) and percentages (C) of TNF-producing macrophages. Macrophages identified as M1 macrophages were characterized as CD206−; M2 macrophages were gated as CD206+. (E–H) Young AL (2 mo) and young *ob/ob* (2 mo) were treated with either control or macrophage depleting clodronate liposomes before and during LD αCD40/IL-2 and survival was monitored; *n* = 5 mice/group. (F and G) On day 2, visceral adipose tissues and peritoneal lavages were collected and assessed for the percentages TNF+ macrophages (F and G) as characterized in experiments in A–D and serum TNF levels (H), *n* = 4 mice/group. (I–L) Young AL (2 mo) and young *ob/ob* (2 mo) mice were treated with either control hIgG/PBS or subcutaneous injection of 1.5 mg/0.1 ml etanercept before and during LD αCD40/IL-2 and survival was monitored (I), *n* = 5 mice/group. (J and K) On day 2, visceral adipose tissue and peritoneal lavages were collected and assessed by flow cytometry for the percentages of TNF+ macrophages (J and K) and serum TNF levels (L); *n* = 4 mice/group. Data in all panels are representative of one of at least three experiments with similar results. Survival data were plotted using the Kaplan-Meier method and statistical differences were determined with the log-rank test. Bar graph (mean value ± SEM) statistics performed using one-way ANOVA with Bonferroni post-hoc tests. **, $P < 0.01$; *, $P < 0.05$.

young WT cohort (Fig. 3 H). 100% of aged AL mice yielded to lethality from the IT by day 2 of treatment, whereas 100% of aged CR mice survived the entire regimen (Fig. 3 H).

The pathological and lethal response observed within the young *ob/ob* mice was not αCD40/IL-2 IT administration specific. Young AL and age-matched young *ob/ob* mice were administered CpG in combination with HD IL-2 and, likewise, resulted in lethality of 75% of young *ob/ob* mice by day 5 of treatment but resulted in complete tolerance by young AL mice (Fig. 3 I). CpG/IL-2 therapy led to significantly increased levels of serum proinflammatory cytokine TNF in an analogous trend as αCD40/IL-2 administration on day 2 of therapy (Fig. 3 J).

This data further supports that increased adiposity plays a crucial role in the induction of systemic toxicities after IT. These data are suggestive that not only does an aging environment result in lethal toxicities but toxicity may also be dependent on the increase in fat accumulation as the young *ob/ob* mice succumb to cytokine storm induction and mortality after IT, similar to that observed in the aged mice.

IT toxicity is TNF– and M1 macrophage–dependent within the peritoneum and visceral adipose tissues

A hallmark of obesity is the increasing infiltration of macrophages into adipose tissues (ATMs) through the secretion of MCP-1 by adipocytes. Phenotypically, these macrophages are
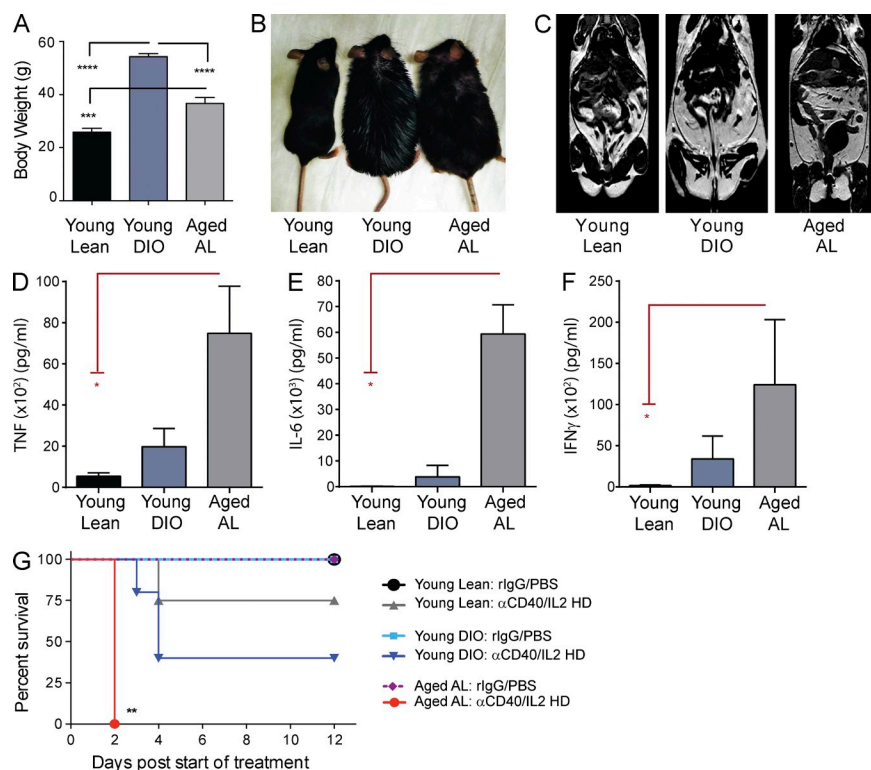
Figure 5. DIO succumb to cytokine storm, organ pathology, and lethality similar to aged AL mice after IT. Young C57BL/6 mice were placed on a 60% fat diet starting at 3 wk of age to induce obesity (young DIO). Lean age-matched controls (young lean) were fed a 10% fat diet beginning at 3 wk of age. Young mice were analyzed at 5 mo of age, and aged AL mice were analyzed at 18 mo of age, n = 6 mice/group. Average body weight (A), representative pictures (B), and total fat content as measured by MRI (C) are shown for each group. (D–F) Young lean (5 mo), young DIO (5 mo), and aged AL (18 mo) mice were treated with HD αCD40/IL-2 or rIgG/PBS. Serum was collected day 2 after the start of treatment and analyzed by CBA for levels of TNF (C), IL-6 (D), and IFN-γ (E) and survival was analyzed (F). Data in A–C are representative of one of at least three experiments with similar results and data in D–G are representative of one of at least four experiments with similar results. Survival data were plotted using the Kaplan-Meier method and statistical differences were determined with the log-rank test. Bar graph (mean value $\pm$ SEM) statistics performed using one-way ANOVA with Bonferroni post-hoc tests. ****, $P < 0.0001$; ***, $P < 0.001$; **, $P < 0.01$; *, $P < 0.05$.

predominately classically activated M1 cells that also express proinflammatory mediators IL-1β, TNF, and IL-6 (Lumeng et al., 2007; Fujisaka et al., 2009). As such, we next sought to determine if increases in M1 macrophages within the peritoneal cavity and visceral adipose tissues could account for the pathological increases in systemic TNF during IT administration. Young AL and age-matched young *ob/ob* mice were administered LD αCD40/IL-2. At day 2 of treatment, visceral adipose tissues and peritoneal lavages were phenotypically assessed by flow cytometry for the presence of M1 (CD206⁻) macrophages, M2 (CD206⁺) macrophages, and percentages of TNF-expressing macrophages. Consistently, young *ob/ob* mice demonstrated significant increases in M1 macrophage proportions during IT administration, whereas young AL mice were able to maintain consistent M1-to-M2 ratios (Fig. 4 A). Additionally, both the visceral adipose tissues and peritoneal lavages of *ob/ob* mice experienced significant increases in percentages of TNF-expressing macrophages as opposed to young AL mice (Fig. 4, B–D). Significant changes were not observed in the spleen of either young *ob/ob* or AL mice (unpublished data). This data, consistent with obesity literature, suggests that increases in adipose tissue accumulation within the visceral cavity may impact regulation of M1 and M2 macrophage ratios that ultimately may affect TNF responses to immune stimulation with immunotherapeutic regimens.

Given the increases in M1 macrophages within the obese mice and dysregulation observed with IT, young *ob/ob* and young AL mice were treated with LD αCD40/IL-2 in conjunction with either liposomal clodronate for macrophage depletion (Fig. 4, E–H) or etanercept (Enbrel) for TNF blockade

(Fig. 4, I–L). Both macrophage depletion and co-treatment with etanercept during LD αCD40/IL-2 resulted in complete protection of young *ob/ob* mice from lethality (Fig. 4, E and I). As expected, treatment with liposomal clodronate led to significantly decreased levels of TNF-producing macrophages within both the visceral fat and peritoneal lavages (Fig. 4, F and G), which significantly reduced systemic circulating serum levels of proinflammatory cytokine TNF (Fig. 4 H). Additionally, co-administration of LD αCD40/IL-2 with etanercept did not reduce the percentages of TNF-expressing macrophages within the visceral fat or peritoneal cavity (Fig. 4, J and K) but mediated complete protection through an overall reduction in systemic TNF levels (Fig. 4 L).

Together, these data indicate that proinflammatory M1 macrophages are the cellular mediator in the induction of IT toxicity, particularly through increased presence within the peritoneal and visceral adipose tissues. Importantly, these effects are TNF-dependent, as blocking TNF levels either through etanercept administration or macrophage depletion resulted in complete protection of young *ob/ob* mice from lethality.

Diet–induced obese (DIO) mice succumb to cytokine storm, organ pathology, and lethality similar to ob/ob and aged AL mice after IT

ob/ob mice are congenic for the spontaneous mutation in the OB gene, resulting in leptin hormone deficiency. To extend our findings, we generated young DIO mice. Mice were placed on a purified 60% fat diet to induce obesity beginning at 3 wk of age and were determined to be obese when weighing >40 g (DIO). Age-matched counterparts were placed on a matching

purified diet that was 10% fat and served as lean controls. Increases in body mass were validated in DIO mice before IT administration (Fig. 5, A–C). DIO mice displayed increases in overall body weight and size (Fig. 5, A and B). MRI analysis of body fat content showed increased total body fat accumulation, largely as increased visceral fat, in young DIO mice that was similar to the aged AL mice (Fig. 5 C).

Confirming our previous findings, DIO mice treated with HD αCD40/IL-2 displayed increased serum TNF, IL-6, and IFN-γ levels compared with age-matched young mice on a 10% fat diet after IT administration (Fig. 5, D–F). The increases in proinflammatory cytokines in DIO mice were lower, yet not significantly so, than aged mice after IT (Fig. 4, C–E). Young DIO mice started succumbing to IT lethality at day 3 of treatment (>60%), and <40% were still alive by day 4 (Fig. 5 G).

Together, these results suggest that adipose tissue is a critical component to the development of systemic cytokine storm and lethality after IT. Yet, due to the observation that treatment of DIO mice did not result in 100% of mice succumbing to lethality, aging itself may also likely contribute to the overall heightened inflammatory responses incurred by IT.

DISCUSSION

After initiation of strong immune stimulation with IT, we show that both young obese and aged AL mice demonstrate increased levels of adiposity, which led to aberrant increases in both TNF and IL-6 levels that ultimately resulted in multiorgan damage. Similar to aging, obesity has been shown to be immunomodulatory, where the cross talk between adipocytes and macrophages is thought to lead toward the development and perpetuation of a meta-inflammatory state through continual NF-κB activation, which is currently hypothesized to be responsible for the induction of metabolic diseases. A study conducted by Spaulding et al. (1997) examined the effects of age and calorie restriction on the production of TNF and IL-6 in resting mice and demonstrated that serum levels of both cytokines were significantly higher in aged mice in comparison to young, and yet aged mice subjected to long-term calorie restriction resulted in TNF and IL-6 serum levels that were comparable to the young mice. These findings lend support to the protective effects seen within our studies in the aged CR cohort administered IT.

Importantly, the data presented here demonstrate the need for using age and body fat content as variables in preclinical assessment of therapeutics and modeling diseases, such as cancer. However, the vast majority of inbred mouse studies are housed in specific pathogen-free colonies where normal aging may result in higher body fat content and yet less immune challenge from pathogens making them more susceptible to proinflammatory responses and toxicities after immune therapies. It will therefore be important that future studies ascertain responses in mice that have been exposed to pathogens and immune challenges as they age.

Furthermore, our data demonstrate that an obese phenotype resulted in lethal consequences that were ameliorated through calorie restriction in the aged. Also, differences in lethality

were observed between young obese and aged AL mice, where aged mice die by day 2 but young obese mice die at day 4 of treatment. Therefore, although our data strongly demonstrates that adiposity plays a central role in the induction of toxicities, aging is also a likely key factor. Therefore, our findings highlight the importance in considering both the status of aging and obesity of patients receiving systemic administration of stimulatory IT regimens. It will be important to conduct studies dissociating the consequences of aging upon increased cytokine responsiveness, possibly through either investigating epigenetic modifications induced by the meta-inflammatory and/or inflammaging states associated with increased adipose accumulation or whether aging is accompanied by changes in expression levels of various receptors that allow for a quicker response.

The development of IT regimens continues on a positive trajectory with increasing successes within a variety of cancers. Active IT has taken a greater comprehensive form focusing on activating humoral and cell-mediated immunity, and these strategies have included antigen-specific vaccines (i.e., MART-1 vaccines), DC-based vaccines (i.e., Sipuleucel-T), inhibitors of checkpoint blockade (i.e., αCTLA-4 and αPD-1), and systemic stimulatory regimens through cytokine based therapies and application of agonistic antibodies (i.e., αCD40, IFN-γ, and IL-2). Our data presented herein demonstrates that both young obese and aged AL mice succumb to rapid lethality during systemic administration of stimulatory therapies. Our data strongly suggests that excess adiposity may be a prognostic factor in determining patient outcome and treatment tolerance. However, additional studies need to be conducted examining the effects of adiposity on the development of adverse reactions within other classes of IT regimens, such as checkpoint inhibitors.

Clinically, we hypothesize that taking into account patient BMI, adipose accumulation, and age may better modulate treatment type choices as well as the inclusion of supportive therapeutics such as TNF blockade in conjunction with anti-cancer therapies that, overall, may increase patient survival and lead to greater anti-cancer responses. Follow-up investigations in tumor-bearing models merit further study.

MATERIALS AND METHODS

Animals and diets. Female young (2–5 mo old), middle-aged (9–12 mo old), and aged (15–22 mo old) C57BL/6 mice were purchased from Charles River or from the animal production area at the National Cancer Institute. Young female B6.Cg-Lep$^{ob/ob}$ and young age-matched female WT control C57BL/6 mice were purchased from The Jackson Laboratory at 8–12 wk of age.

DIO obese and control lean mice were generated from WT C57BL/6 mice purchased at 3 wk of age from Charles River or from the animal production area at the National Cancer Institute. Mice were placed on an open-source purified diet consisting of either 60% high-fat (D12492) or 10% low-fat (D12450J) constitution (Research Diets, Inc.). Age-matched mice were placed on either a high-fat or low-fat diet beginning at 3 wk of age for 16–20 wk and weighed weekly. Mice were deemed obese upon reaching a minimum of 40 g of weight.

For studies comparing aged AL and CR dietary effects, both female aged CR and age-matched female AL-littermates (15–22 mo old) were purchased from the CR rodent colony at the National Institutes on Aging, National Institutes of Health (NIH). In brief, mice were either raised through free access, AL, feeding on the NIH31 regular chow, or placed on a limited daily feeding

Table 1. Grading of acute liver damage

Global assessment	Criteria
0: None	No portal inflammation
I: Minimal/indeterminate	Portal inflammatory infiltrate is in a minority of the portal triads, which is minimal
II: Mild	Inflammatory infiltrate in 50% of the triads, which is generally mild, and confined within the portal spaces
III: Moderate	Inflammatory infiltrate, expanding most or all of the triads, and associated with mild interface and lobular activity
IV: Severe	As above for moderate, with spillover into periportal areas and moderate to severe perivenular inflammation that extends into the hepatic parenchyma and is associated with perivenular hepatocyte necrosis

schedule with the NIH31-fortified chow. CR is initiated at 14 wk of age at 10% restriction, increased to 25% restriction at 15 wk, and to 40% restriction at 16 wk of age where it is maintained throughout the life of the animal. Information on survival curves, food intake curves, and body weights of the NIA strains has been previously published (Turturro et al., 1999).

All experimental mice were housed in the Animal Facilities at the University of California, Davis under specific pathogen-free (SPF) conditions. For the comparison in fat volume ratios, young, middle-aged, and aged AL and CR mice were ordered and sent to the National Institute on Aging for MRI analysis and also housed under SPF conditions. All of the animal protocols were approved by the Institutional Animal Care and Use Committees of both institutions. Body weights were also measured for several mice at different ages and on dietary regimens. Mice were euthanized by CO_2 asphyxiation and the visceral fat pads (mesenteric, gonadal, and renal) were collected and weighed together for each mouse to determine the visceral fat weight.

Reagents. The agonistic anti–mouse CD40 antibody (clone FGK115B3) was generated via ascites production in our laboratory as previously described (Murphy et al., 2003; Bouchlaka et al., 2013). The endotoxin level of the αCD40 was <1 endotoxin unit/mg of antibody as determined by a quantitative chromogenic limulus amebocyte lysate kit (QCL-1000; Bio Whittaker). Recombinant human IL-2 (rhIL-2; TECIN Teceleukin) was provided by the National Cancer Institute (NCI). Murine CpG ODN 1826 was purchased from InvivoGen. All were injected i.p.

Schedule of αCD40/IL-2 and CpG/IL-2 IT treatments. Mice were treated with agonist αCD40 antibody and rhIL2 as previously described (Murphy et al., 2003; Bouchlaka et al., 2013). αCD40 or CpG was administered daily for a total of 5 consecutive days (days: 0, 1, 2, 3, and 4) and IL-2 was administered twice a day for a total of 4 d (days: 1, 4, 8, and 12). Control mice received rat IgG (rIgG; Jackson ImmunoResearch Laboratories, Inc.) and PBS (Cellgro). Survival was monitored daily. An HD or LD of αCD40/IL-2, or HD CpG/IL-2, was administered as follows on the same scheduling pattern as previously described (Bouchlaka et al., 2013): HD αCD40/IL-2, mice received 80 µg of agonist αCD40 and 10^6 IU of IL-2 in 0.2 ml PBS i.p.; control mice received 80 µg rIgG in PBS; LD αCD40/IL-2, mice received 40 µg of agonist αCD40 and 4×10^5 IU of IL-2 in 0.2 ml PBS i.p; control mice received 40 µg rIgG in PBS; CpG/HD IL-2, mice received 100 µg CpG ODN 1826 (InvivoGen) and 10^6 IU of IL-2 in 0.2 ml PBS i.p.

Macrophage depletion and TNF blockade with etanercept (Enbrel). In some experiments, mice were in vivo depleted of macrophages using liposomal clodronate or control-loaded liposomes (Encapsula NanoScience) before and during IT administration, as previously described (Bouchlaka et al., 2013). For experiments where mice were euthanized by day 2 of treatment, 0.2 ml per dose was injected i.p. of either clodronate or control liposomes on days −2 and 0. For all survival experiments, clodronate or control liposomes were administered on days −2, 0, 2, and 4.

TNF blockade was preformed through in vivo subcutaneous injection of 1.5 mg/0.1 ml etanercept (Enbrel) on days −1 and 1 for experiments where mice were euthanized on day 2 of IT therapy. For all survival experiments, etanercept was administered on days −1, 1, 3, 7, and 9.

Murine macrophage studies. On day 2 of treatment, murine macrophages were isolated from either the peritoneal cavity or visceral adipose tissue. For peritoneal lavages, 4 ml of cold PBS was injected into the peritoneal cavity of each mouse and then aspirated. Lavages were spun down at 1,200 rpm for 5 min and the resulting pellet was resuspended in RF10c media and plated for flow cytometry staining.

The stromal vascular fraction of visceral adipose tissues was collected day 2 of treatment. Adipose tissues from the visceral cavity (gonadal) were collected and then incubated for 60 min in a digestion solution consisting of 2 mg/ml type IV collagenase (Sigma-Aldrich) dissolved fresh in a 2% BSA in PBS solution. After incubation samples were centrifuged at 1,200 rpm for 5 min for layer separation of the stromal vascular fraction from adipocytes. The resulting stromal vascular fraction was then removed, resuspended into a single cell suspension, counted, and plated for flow cytometry staining.

Flow cytometry analysis of macrophages. Single cell suspensions from the peritoneal lavages and visceral adipose tissues were plated in RF10c media with the addition of GolgiPlug (containing Brefeldin A) and GolgiStop (containing Monensin) Protein Transport Inhibitors (BD) according to manufacturer's protocols. Plates were incubated for 9 h at 37°C and 5% CO_2.

After incubation, cells were washed with PBS and stained for flow analysis. Single cell suspensions were labeled with Fc block (purified anti–mouse CD16/32; BD) for 10 min, followed by labeling with antibodies for 20 min at 4C. Cells were washed twice with a staining buffer consisting of 5% FBS (Gemini Bio-products) in DPBS (Corning). For intracellular staining, the Cytofix/Cytoperm kit (BD) was used per manufacturer's protocols. After staining, cells were analyzed using a custom configured Fortessa cytometer, and by using FACSDiva software (BD). Data were analyzed using FlowJo software vX (Tree Star). Antibodies used to distinguish macrophages were: PB-conjugated anti–mouse CD45, BV711-conjugated anti–mouse CD11b, BV605- and PE-conjugated anti–mouse CD206, BV785-conjugated anti–mouse CD19, APC-conjugated anti–mouse F4/80, and PE-Cy7–conjugated anti–mouse TNF (BioLegend).

Serum cytokine bead array. Serum levels of TNF, IFN-γ, and IL-6 were quantified by multiplex measurement using the Cytometric Bead Array (CBA; BD) kit as described previously (Bouchlaka et al., 2013). In brief, serum samples and standards were incubated for 1 h at 25°C with a bead mixture containing bound antibodies to TNF, IFN-γ, and IL-6 according to manufacturer's instructions. Samples and standards were resuspended in wash buffer and analyzed by flow cytometry. Data were acquired on a custom-configured Fortessa cell analyzer using FACSDiva software (BD) and analyzed using FlowJo software (Tree Star). Each sample was analyzed in triplicate. Upon analysis of raw data, the mean fluorescent intensities (MFIs) of each bead cluster were quantified. Where indicated in the figures, protein concentrations were extrapolated relative to a standard curve created by serial dilution of the mouse positive control cytokine.

Colorimetric liver enzyme assay. Serum ALT was quantified using the ID Labs ALT Enzymatic Assay kit (ID Labs Biotechnology Inc.) as previously described (Bouchlaka et al., 2013). Colorimetric determination of ALT levels was performed by reading the absorbance of each well at 340 nm on a plate reader (VERSAmax turntable plate reader). The concentration of ALT (U/liter)

Table 2. Grading of acute intestinal damage

Global assessment	Criteria
0: None	No inflammation
I: Minimal/indeterminate	Scattered infrequent inflammatory infiltrate in a minority of crypts, which is minimal
II: Mild	Inflammatory infiltrate in 50% of the crypts, which is generally mild, and confined within the mucosa epithelium with mild architectural distortion
III: Moderate	Inflammatory infiltrate involving most of the crypts, and associated with architectural distortion (villous blunting and focal mucosal atrophy/erosion) and luminal inflammatory exudate
IV: Severe	Extensive inflammatory infiltrate (large lymphoid aggregates) with expanding into the lamina/muscular propria, and associated with prominent mucosal ulceration/denuding, muscular wall necrosis, and/or perforation

in each sample was then directly determined from the change in absorbance within 5 min time. Dilutions of the Pyruvate Control, included in the kit, were used to construct a standard curve to calibrate the assay. Every serum sample was assayed in triplicate.

Histopathology and grading/scoring. Liver and whole intestines were collected on day 2 of IT, flushed, and fixed in 10% paraformaldehyde, embedded in paraffin, cut into 5-µm sections, and stained with hematoxylin and eosin (H&E). All tissues were prepared and stained at Histology Consultation Services, Inc. (Everson, WA). Images were captured with a microscope (BX4; Olympus) equipped with a Q-color3 camera and 10× numerical aperture objective lens. Magnification for each captured image is specified in the figure legends. Grading of histopathological inflammation was performed using a scale from 0 to 4 in a blind fashion by a board-certified pathologist (M. Chen) at the UC Davis Medical Center's Department of Pathology and Laboratory Medicine. Specifically, the grading score for liver and gastrointestinal tract followed our previously published grading method (Bouchlaka et al., 2013), summarized in Tables 1 and 2.

MRI. To quantify abdominal fat, MR images were acquired in collaboration with the National Institute on Aging. Images were acquired using a Biospec 7 Tesla 30-cm MRI scanner (Bruker Biospin) with a 72-mm diameter transmit-receive birdcage coil. In each experiment, two mice were inserted into the scanner, side by side, in feet-first prone orientation immediately after sacrifice. During scanning, the mice were cooled with a stream of cold air from a vortex tube (Exair, Inc.) to minimize decomposition. Two different pulse sequences were used: a heavily T1-weighted fast spin echo (RARE) sequence yielding bright-fat (water-suppressed [WS]) images and a fat-suppressed proton density weighted fast gradient echo (FLASH) sequence yielding fat-suppressed (FS) images. 3D datasets were acquired in axial orientation with a field of view of 72 × 36 × 80 mm (left-right × anterior-posterior × head-foot) and matrix size 256 × 128 × 128. The voxel size (spatial resolution) was 281 × 281 × 625 µm. The spectral bandwidth in both sequences was 100 kHz (391 Hz/pixel) and two averages were acquired for improved signal-to-noise ratio. For the RARE sequence, the RARE factor (i.e., number of spin echoes per shot or number of k-space lines per segment) was 8, the repetition time (TR) was 125 ms, the actual echo time (TE) was 11.4 ms, and the effective echo time (TEeff) was 46.3 ms. Each RARE scan took 8 min and 32 s to acquire. For the FLASH sequence, the repetition time was 25 ms and the echo time was 3.2 ms. The excitation pulse had a flip angle of 30°. Each FLASH scan took 13 min 39 s to acquire. Image processing was performed in ImageJ 1.45 (NIH). The statistical analyses were performed using one-way ANOVA and the Newman-Keuls post-hoc test. P < 0.05 was considered to be significant.

To visualize fat distribution and content imaging of young *ob/ob*, DIO, and lean age-matched controls were conducted in collaboration with the Center for Molecular and Genomic Imaging (CMGI) Facility at the University of California, Davis. Mice were anesthetized before imaging using 2% isoflurane in an induction chamber and then maintained on 1–2% isoflurane throughout imaging via a nose cone fitted for anesthetic inhalation. Mice were imaged using a BioSpec 70/30 7T (Bruker Biospin) horizontal bore system designed specifically for small animal imaging. Animals were kept at normal body temperature using warm air. Mice were inserted into the scanner in a head-first prone orientation. Spin-echo T1-weighted images were obtained through the mouse body (neck-to-base of the tail) using a 72-mm linear volume coil. Scan sequence parameters were the following: TR 1,000 ms, TE 15 ms, and 2 averages. The field of view was 7.7 × 3.85 × 2.0 cm, with a matrix size of 256 × 128 × 40. The corresponding voxel size was 0.3 × 0.3 × 0.5 mm. Images were acquired using ParaVision 5.0 software. After acquisition, images were transferred into Invenon Research Workplace 4.0 software (Siemens Preclinical) allowing fat to be displayed with high intensity (white).

Statistical analysis. Statistical analyses were performed using Prism software (GraphPad Software Inc.). Data were expressed as mean ± SEM. For analysis of three or more groups, a nonparametric ANOVA test was performed with a Bonferroni post-hoc test. Analysis of differences between two normally distributed test groups was performed using the Student's *t* test. Non-parametric groups were analyzed with the Mann-Whitney test. Welch's correction was applied to datasets with significant differences in variance before Student's *t* test.

Author contributions: A. Mirsoian, M.N. Bouchlaka, D.D. Taub, and W.J. Murphy designed the research; A. Mirsoian, M.N. Bouchlaka, G.D. Sckisel, M. Chen, C.C.S. Pai, A.M. Monjazeb, and D.D. Taub performed the research; A. Mirsoian, M.N. Bouchlaka, D.D. Taub, and W.J. Murphy analyzed the data; M. Chen analyzed and scored all histology data; E. Maverakis provided etanercept (Enbrel) for TNF blockade studies; R.G. Spencer, K.W. Fishbein, and S. Siddiqui performed and analyzed MRI studies; B. Martin, C. Hesdorffer, L. Ferrucci, and S. Maudsley provided aged mice and assisted with data interpretation; A. Mirsoian, M.N. Bouchlaka, D.D. Taub, and W.J. Murphy wrote the paper; and G.D. Sckisel, D.L. Longo, B.R. Blazar, and R.H. Wiltrout helped with the editing of the paper. All authors read and approved the manuscript.

REFERENCES

Ailhaud, G. 2000. Adipose tissue as an endocrine organ. *Int. J. Obes. Relat. Metab. Disord.* 24:S1–S3. http://dx.doi.org/10.1038/sj.ijo.0801267

Balducci, L., and W.B. Ershler. 2005. Cancer and ageing: a nexus at several levels. *Nat. Rev. Cancer.* 5:655–662. http://dx.doi.org/10.1038/nrc1675

Bouchlaka, M.N., G.D. Sckisel, M. Chen, A. Mirsoian, A.E. Zamora, E. Maverakis, D.E. Wilkins, K.L. Alderson, H.H. Hsiao, J.M. Weiss, et al. 2013. Aging predisposes to acute inflammatory induced pathology after tumor immunotherapy. *J. Exp. Med.* 210:2223–2237. http://dx.doi.org/10.1084/jem.20131219

Campisi, J. 2013. Aging, cellular senescence, and cancer. *Annu. Rev. Physiol.* 75:685–705. http://dx.doi.org/10.1146/annurev-physiol-030212-183653

Franceschi, C. 2007. Inflammaging as a major characteristic of old people: can it be prevented or cured? *Nutr. Rev.* 65:S173–S176. http://dx.doi.org/10.1111/j.1753-4887.2007.tb00358.x

Franceschi, C., M. Bonafè, S. Valensin, F. Olivieri, M. De Luca, E. Ottaviani, and G. De Benedictis. 2000. Inflamm-aging. An evolutionary perspective on immunosenescence. *Ann. N.Y. Acad. Sci.* 908:244–254. http://dx.doi.org/10.1111/j.1749-6632.2000.tb06651.x

Fujisaka, S., I. Usui, A. Bukhari, M. Ikutani, T. Oya, Y. Kanatani, K. Tsuneyama, Y. Nagai, K. Takatsu, M. Urakaze, et al. 2009. Regulatory mechanisms for adipose tissue M1 and M2 macrophages in diet-induced obese mice. *Diabetes*. 58:2574–2582. http://dx.doi.org/10.2337/db08-1475

Harris, T.B. 2002. Invited commentary: body composition in studies of aging: new opportunities to better understand health risks associated with weight. *Am. J. Epidemiol.* 156:122–124, discussion :125–126. http://dx.doi.org/10.1093/aje/kwf024

Lee, S., and K. Margolin. 2011. Cytokines in cancer immunotherapy. *Cancers (Basel)*. 3:3856–3893. http://dx.doi.org/10.3390/cancers3043856

Lumeng, C.N., S.M. Deyoung, J.L. Bodzin, and A.R. Saltiel. 2007. Increased inflammatory properties of adipose tissue macrophages recruited during diet-induced obesity. *Diabetes*. 56:16–23. http://dx.doi.org/10.2337/db06-1076

Murphy, W.J., L. Welniak, T. Back, J. Hixon, J. Subleski, N. Seki, J.M. Wigginton, S.E. Wilson, B.R. Blazar, A.M. Malyguine, et al. 2003. Synergistic anti-tumor responses after administration of agonistic antibodies to CD40 and IL-2: coordination of dendritic and CD8^{+} cell responses. *J. Immunol.* 170:2727–2733. http://dx.doi.org/10.4049/jimmunol.170.5.2727

Ronti, T., G. Lupattelli, and E. Mannarino. 2006. The endocrine function of adipose tissue: an update. *Clin. Endocrinol. (Oxf.)*. 64:355–365.

Spaulding, C.C., R.L. Walford, and R.B. Effros. 1997. Calorie restriction inhibits the age-related dysregulation of the cytokines TNF-alpha and IL-6 in C3B10RF1 mice. *Mech Ageing Dev.* 93:87–94. http://dx.doi.org/10.1016/S0047-6374(96)01824-6

Turturro, A., W.W. Witt, S. Lewis, B.S. Hass, R.D. Lipman, and R.W. Hart. 1999. Growth curves and survival characteristics of the animals used in the Biomarkers of Aging Program. *J. Gerontol. A Biol. Sci. Med. Sci.* 54:B492–B501. http://dx.doi.org/10.1093/gerona/54.11.B492

Vázquez-Vela, M.E., N. Torres, and A.R. Tovar. 2008. White adipose tissue as endocrine organ and its role in obesity. *Arch. Med. Res.* 39:715–728. http://dx.doi.org/10.1016/j.arcmed.2008.09.005

Yang, H., Y.H. Youm, B. Vandanmagsar, J. Rood, K.G. Kumar, A.A. Butler, and V.D. Dixit. 2009. Obesity accelerates thymic aging. *Blood*. 114:3803–3812. http://dx.doi.org/10.1182/blood-2009-03-213595